Web-based Histology Reference Atlas for the Freshwater Crustacean *Daphnia magna*

[1,2]Mee S. Ngu, [1,2]Daniel J. Vanselow, [1,2]Carolyn R. Zaino, [1,2]Alex Y. Lin, [1,2]Jean E. Copper, [3]Margaret J. Beaton, [4]John K. Colbourne, [1,2]Keith C. Cheng✉, [1,2]Khai C. Ang✉

[1]Department of Pathology, Pennsylvania State University College of Medicine, Pennsylvania, USA

[2]Jake Gittlen Laboratories for Cancer Research, Pennsylvania State University College of Medicine, Pennsylvania, USA

[3]Department of Biology, Mount Allison University, Sackville, Canada

[4]School of Biosciences, The University of Birmingham, Birmingham, UK

✉Corresponding authors: kca2@psu.edu, kcheng76@gmail.com

Abstract

Daphnia, an important model system for the study of evolution, development, phenotypic plasticity, and environmental health, lacks a modern reference atlas for microanatomy. To facilitate the comprehensive assessment of phenotypic effects of genes and environment, we created the histology reference atlas for *Daphnia* (http://daphnia.io/anatomy/), a tractable, ok, interactive web-based tool that provides insight into normal phenotype through vectorized annotations overlaid onto digital histology sections imaged at 40X magnification. Guided by our expert-curated and multimodal informed hierarchical anatomical ontology, we show that this resource can be used to elucidate sex-specific differences of female and male *Daphnia magna* in each of 3 orthogonal planes, providing new insight for the study of sex-specific traits. It is our intention that this atlas aids in phenotypic anchoring of large-scale biomolecular (multi-omics) data from comparative toxicological studies. Greater access to high-quality histological data may clarify cross-correlations between microanatomic and multi-omic phenotypes caused by genetic variation, environment, and disease across phylogeny.

1. Introduction

Keystone species of freshwater ecosystems (algae, zooplankton, fish) forming a food chain are used in ecotoxicology as sentinels to monitor water quality, to manage chemical risks to the

environment, and to serve as early warning signs of chemical health hazards that can cause human disease (Au, 2004). Histopathology permits the identification of cell- and tissue-specific changes in whole organisms, making it a powerful tool for detecting the adverse effects of toxicants. Multiple histopathology-based toxicological screens using fish (Bernet et al., 1999; Ramírez-Duarte et al., 2008; Wester and Vos, 1994) and aquatic invertebrates (Chakraborty et al., 2010; LaDouceur et al., 2016) have been reported. Ideally, the evaluation of toxic effects of chemicals, environmental contaminants, and pollutants identifies all affected cell types and organ systems so that the mechanisms underlying adverse outcomes and disease can be accurately predicted and better understood. However, identification of these toxic effects requires prior knowledge of normal structure, which can be most readily facilitated through atlases in the field of medicine and comparative biology. Atlases provide a systematic approach for understanding the anatomical and histological context of all cells and tissues in both normal and diseased states. Reference atlases of various model organisms (e.g., zebrafish at http://bio-atlas.com/zebrafish/ and *Caenorhabditis elegans* at www.wormatlas.org) serve as valuable resources for the research community and the public.

Daphnia, a branchiopod micro-crustacean, is one of the most abundant zooplankters of lentic ecosystems around the globe and a model system in the fields of ecology and evolution (Lampert, 2011; Stollewerk, 2010). *Daphnia magna* primarily inhabit freshwater environments throughout the Northern Hemisphere and South Africa yet are distributed to laboratories around the globe as an established invertebrate model in ecotoxicology. It is sensitive to environmental contaminants, which impact its growth, reproduction, mobility, and mortality (Kikuchi et al., 2000; Kühn et al., 1989; Tkaczyk et al., 2021). It has been widely used as an indicator of water quality, assigned a role in setting regulatory criteria for toxicity testing by government agencies worldwide (Environmental Protection Agency, 2002, 1996; OECD, 2018, 2004), and has assumed a central role in ecotoxicogenomics (Kim et al., 2015; Shaw et al., 2008). Its extensive utilization for toxicological studies makes it important to establish a comprehensive reference atlas to enable whole-organism phenotyping and characterization of the full range of cellular and molecular phenotypic responses to environmental contaminants.

Here, we present a web-based histology reference atlas of *D. magna*, with an interactive viewer that enables visualization of images up to 40X magnification and highlighting of anatomical structures with corresponding labels. This atlas allows for visualization of differences between males and females that are dimorphic clones (Hebert and Ward, 1972; Kvist et al., 2020) produced parthenogenetically from the same mother. This atlas will serve as a framework for a non-targeted approach to assess the toxicological phenotypic effects of pollutants that complement non-targeted biomolecular approaches at discovering toxicity pathways, thereby enabling a fuller understanding of the causal links to adversity using sentinel organisms.

2. Results and Discussion

The creation of the *Daphnia* histology reference atlas involved designing a casting mold to ensure consistency in sample orientation for histology sectioning in any of the three orthogonal orientations, optimizing sample preparation and staining for histology, labeling and digital segmentation of anatomical structures, and constructing a web interface for the presentation of histological data and annotation.

2.1 Triangle casting mold for agarose pre-embedding

Precise and consistent orientation of samples in paraffin is critical for achieving near orthogonal alignment. To this end, samples were pre-embedded in agarose blocks prior to downstream tissue processing for paraffin embedding. Specialized casting molds were engineered for this study to produce agarose blocks with wells that house individual *Daphnia* samples. Casting molds with three different teeth designs: sloped rectangle, triangle, and rectangle, were tested for efficacy (Supplemental Figure 1, see Supplements for discussions). The dimensions of each mold (24 mm X 29 mm) are slightly smaller than the tissue cassettes (27 mm X 31mm) used for tissue processing. Molds were printed using stereolithography (3D-SLA). 3D-SLA printing at 25 µm resolution creates a smooth surface for the mold, allowing the agarose block to be peeled off easily. Spacing of 1 mm between teeth ensured adequate rigidity between wells, while mold thickness of at least 4 mm provided an adequate surface for taping to hold molten agarose. Embedding trials with different casting molds concluded that "triangle mold" with teeth length of 4.5 mm, and height and width of 1.5 mm (Figure 1A-B, STL file in Supplement File 1) allowed precise positioning of *D.*

magna samples with ease and yielded consistent orthogonal orientation of histological sections (Figure 1G).

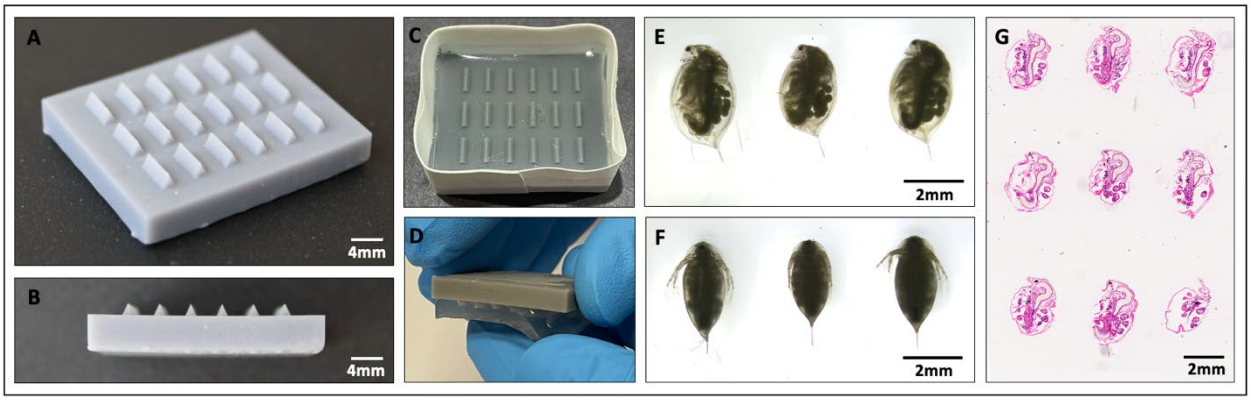

Figure 1. Agarose embedding using casting mold for histological processing. (A) Top view and **(B)** side view of "triangle mold" printed by stereo-lithography (3D-SLA). **(C)** Casting 1% agarose block in the taped mold. **(D)** Agarose block being removed from the mold after solidification by peeling the gel downwards. **(E)** *Daphnia magna* samples were laid on their sides with a swimming antenna in the wells, the rostra facing the same direction for sagittal plane sectioning, and **(F)** laid on their back in the wells for coronal and transverse plane sectioning. **(G)** The histological section showed the position of samples at a similar plane.

2.2 Bouin's is a fixative of choice for *Daphnia* histology

The accurate representation of histological microanatomy depends upon the preservation of tissue structure with minimal distortion and optimal staining that allows a clear distinction between different cell types and subcellular structures. Chemical reactions between fixatives and biological tissue result in distortions known as fixation artifacts. To minimize these artifacts, we evaluated the effectiveness of three common fixatives; Bouin's solution, 4% Paraformaldehyde (PFA), and 10% Neutral Buffered Formalin (NBF), and assessed changes in tissue volume and architecture, the extent of tissue preservation, and clarity of cell boundaries. Histology sections of *D. magna* samples fixed with Bouin's solution at room temperature for 48 hours showed the best fixation and nuclear clarity. Preservation by Bouin's solution provided clearer cell boundaries that allowed easier distinction between nerve fibers and cells in the optic lobe (OL) and cerebral ganglion (CG) (Figure 2A). Poor fixation is commonly encountered in the gut, presumably due to the presence of digestive enzymes (Copper et al., 2018). Bouin's solution resulted in good gut fixation where microvilli were present along the majority of the intestinal lumen and nucleoli in the gut epithelial cells were also more distinct (Figure 2B Inset). Nurse cells and yolk granules were more intact in

120 the ovaries (Figure 2C), and cellular features across the developing embryos are generally more
121 distinct (Figure 2D). Overall, Bouin's solution provided consistent fixation throughout the whole
122 sample and yielded good preservation across tissue and cell types (see Supplemental Figure 3 for
123 the result of fixation by 4% PFA and 10% NBF).
124

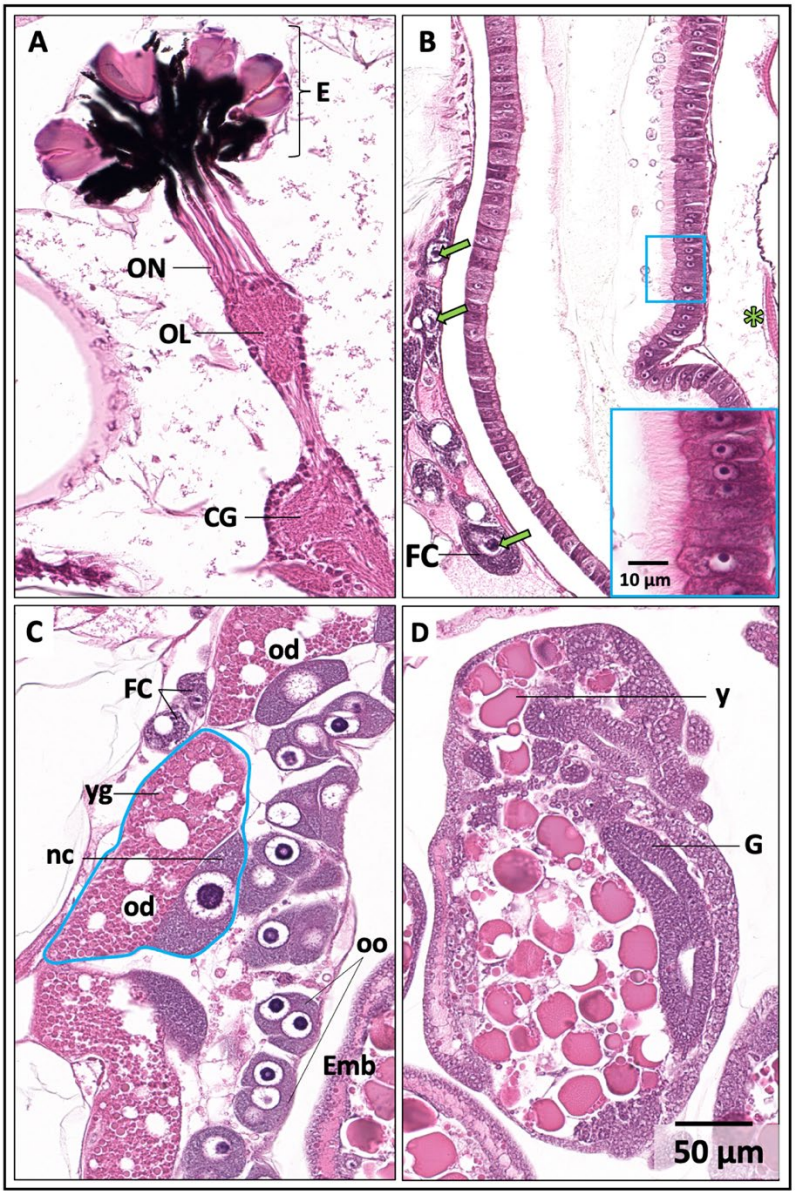

125

126 **Figure 2. Fixation by Bouin's solution allows visualization of cellular details across**
127 **anatomical structures**: **(A)** nerve fibers and cells in the optic lobe (OL) and cerebral ganglion
128 (CG), **(B)** microvilli and nucleoli of the epithelial cells (inset) in the midgut, nucleoli in the fat
129 cells (FC) (arrows) and muscle striations (asterisk), **(C)** yolk granules (yg) and nurse cell (nc) in
130 an ovarian egg (outlined in blue), and **(D)** developing embryo in the brood chamber. Emb, embryo;
131 G, gut precursor; od, oil droplet; oo, oocytes.

132 2.3 Interactive web-based viewer for the *Daphnia* histology reference atlas

133 The *Daphnia* histology reference atlas (http://daphnia.io/anatomy/) presents 40X magnification
134 digital scans of ~5 µm thick histological sections generated from serially sectioned *D. magna* of
135 both sexes in three orthogonal planes (sagittal, coronal, and transverse). The atlas includes an
136 interactive, high-resolution viewer with an anatomical ontology (a list of terms organized by
137 groups and subgroups), color-coded based on organ systems. In the viewer, anatomical ontology
138 is listed on the left, in a hierarchical tree that can be expanded and collapsed (Figure 3). A check
139 in the checkbox indicates that the structure is labeled with a corresponding color overlay.
140 Structures with underlined labels indicate at least one nested substructure (for example,
141 "microvilli" under "epithelial cell", both under "midgut"). Hovering over a structure dynamically
142 highlights the corresponding structure or structure groups in the viewer, temporarily hiding other
143 checked structures. The search function is available to find any structure in the list. In the image
144 portion of the viewer, all available color overlay and acronym labels are on display by default
145 (indicated by checked checkboxes) (Figure 3). Hovering the mouse cursor over a colored region
146 on the image will display its full name. Clicking on the colored region will change the colored
147 overlay to highlight the border only. While images with interactive highlighting of anatomical
148 structures assist in structure identification, additional unannotated images of serially sectioned *D.*
149 *magna* are categorized under 'Full Series'. A list of literature and glossary are included under
150 References and Resources, respectively, to provide users quick access to additional information.
151

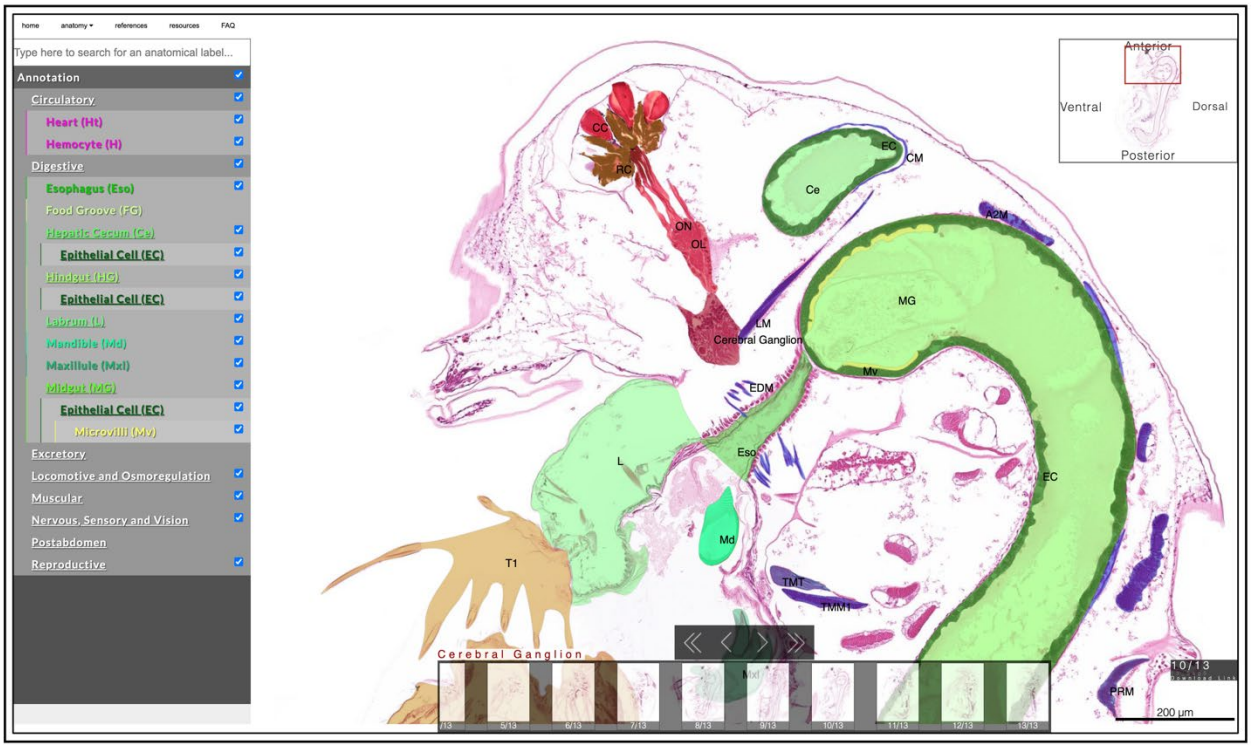

Figure 3. Overview of the interactive web-based viewer for *Daphnia* histology reference atlas. The left pane of the viewer includes an expandable hierarchical tree of anatomical structures; the checked boxes indicate which structures are labeled in the image. The image shows acronym labels; hovering the mouse cursor over an acronym or its corresponding region will bring up the structure's full name. Unchecking a box will eliminate the corresponding color overlay and annotation. These features are demonstrated in a movie clip (Supplemental File 2).

2.4 *Daphnia magna* anatomy

The anatomy and physiology of *Daphnia* have been studied since the early 1800s. To ensure consistency and relevance to current research, we cross-referenced these published materials with our images to provide a visualization platform of various anatomical features (Agar, 1950; Auld et al., 2010; Beaton and Hebert, 1989; Bednarska, 2006; Benzie, 2005; Binder, 1931; Christensen et al., 2018; Consi et al., 1987; Edwards, 1980; Fryer, 1991; Goldmann et al., 1999; Halcrow, 1976; Hiruta and Tochinai, 2014; Kikuchi, 1983; Kress et al., 2016; McCoole et al., 2011; Metschnikoff, 1884; Rossi, 1980; Schultz and Kennedy, 1976; Smirnov, 2017; Stein et al., 1966; Steinsland, 1982; Quaglia et al., 1976; Weiss et al., 2012; Wuerz et al., 2017; Zaffagnini and Zeni, 1986, 1987; Zeni and Franchini, 1990). Representative images from each of the three orthogonal planes (sagittal, coronal, and transverse) showing the most anatomical structures of female (Figure 4-6) and male (Figure 7-9) are presented below with a brief description and links to the atlas.

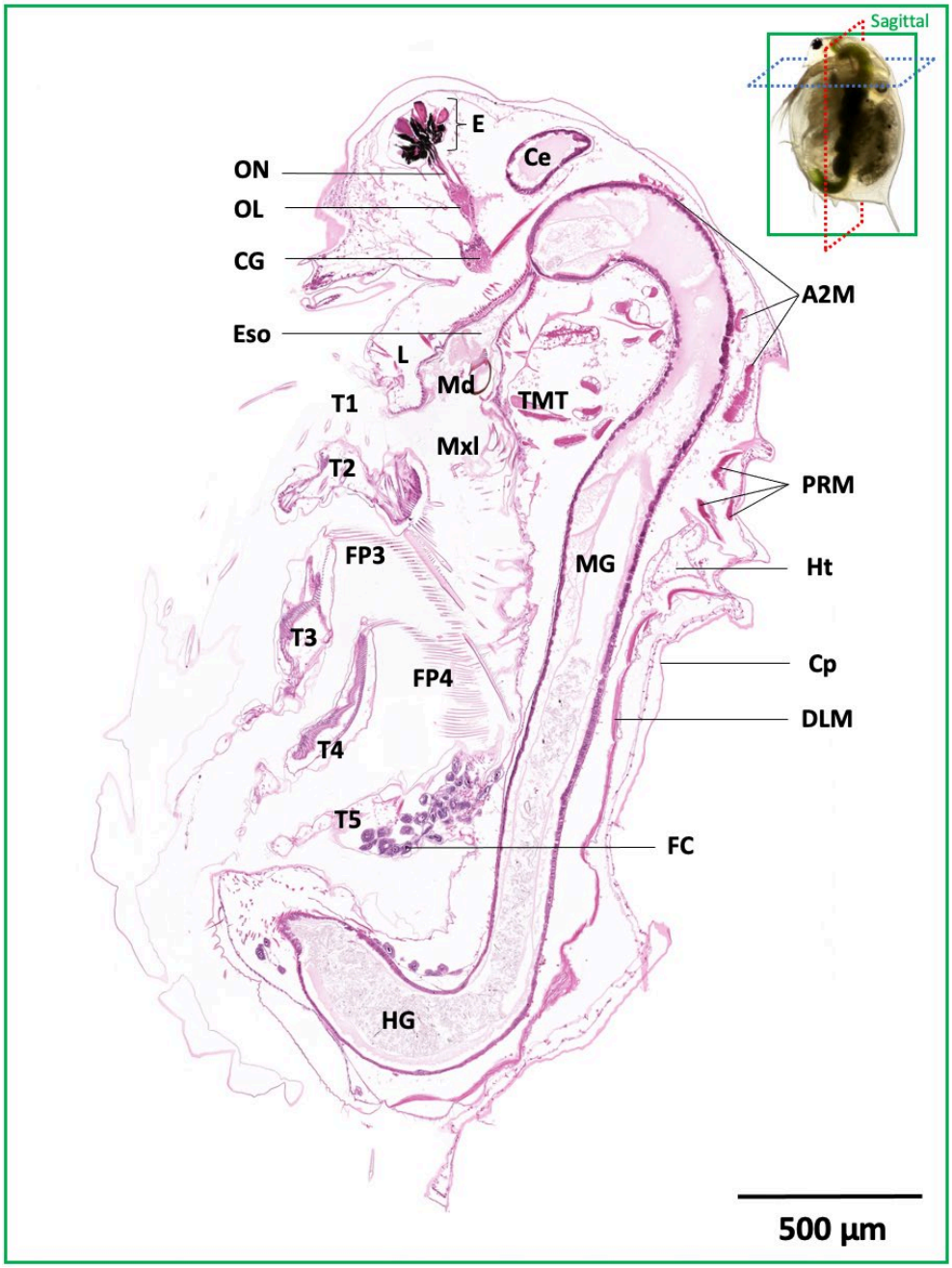

Figure 4. Representative image showing anatomical structures of female *D. magna* in the sagittal plane. The sagittal plane at the approximate median section displays the connection of compound eye (E) to optic lobe (OL) and cerebral ganglion (CG) by optic nerves (ON). The labrum (L), maxillule (Mxl), and mandible (Md) are anterior to the esophagus (Eso) that opens into the midgut (MG) and is followed by the hindgut (HG). This section also cuts through the five thoracic limbs (T1-5) with filter plates (FP3, FP4), the antennal muscles (A2M), the posterior rotator muscle of mandibles (PRM), the heart (Ht), and shows the extent of dorsal longitudinal muscle (DLM) along the gut. Other features seen include the carapace (Cp), hepatic cecum (Ce), fat cells (FC), and transverse mandibular tendon (TMM). Corresponding atlas link: http://daphnia.io/anatomy/histology/?t=sagittal_female&z=10

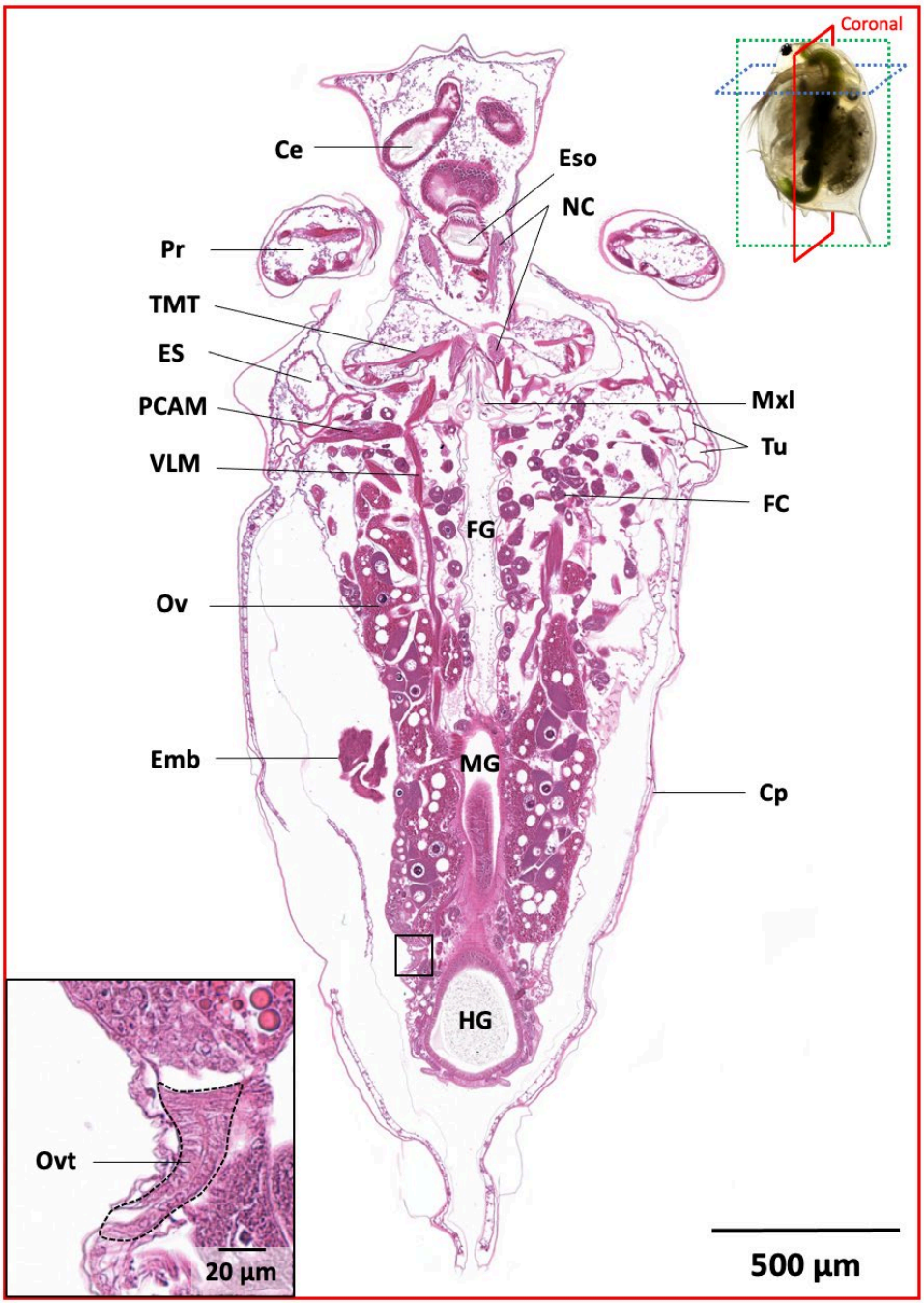

Figure 5. Representative image showing anatomical structures of female *D. magna* in the coronal plane. The coronal plane displays most of the structures in pairs, for example, the protopodites (Pr) of the swimming antennae, hepatic ceca (Ce), maxillules (Mxl), nerve cords (NC), transverse mandibular tendons (TMT), ovaries (Ov), and ventral longitudinal muscles (VLM). It also shows the food groove (FG) that channels food to the maxillules. Other features seen include the carapace (Cp), the end sac (ES) and tubules (Tu) of the maxillary gland, the midgut (MG), the abundant fat cells (FC), the hindgut (HG), and a portion of an embryo (Emb) in the brood chamber. Inset showing the oviduct (Ovt; dotted circle). Corresponding atlas link: https://daphnia.io/anatomy/histology/?t=coronal_female&z=10

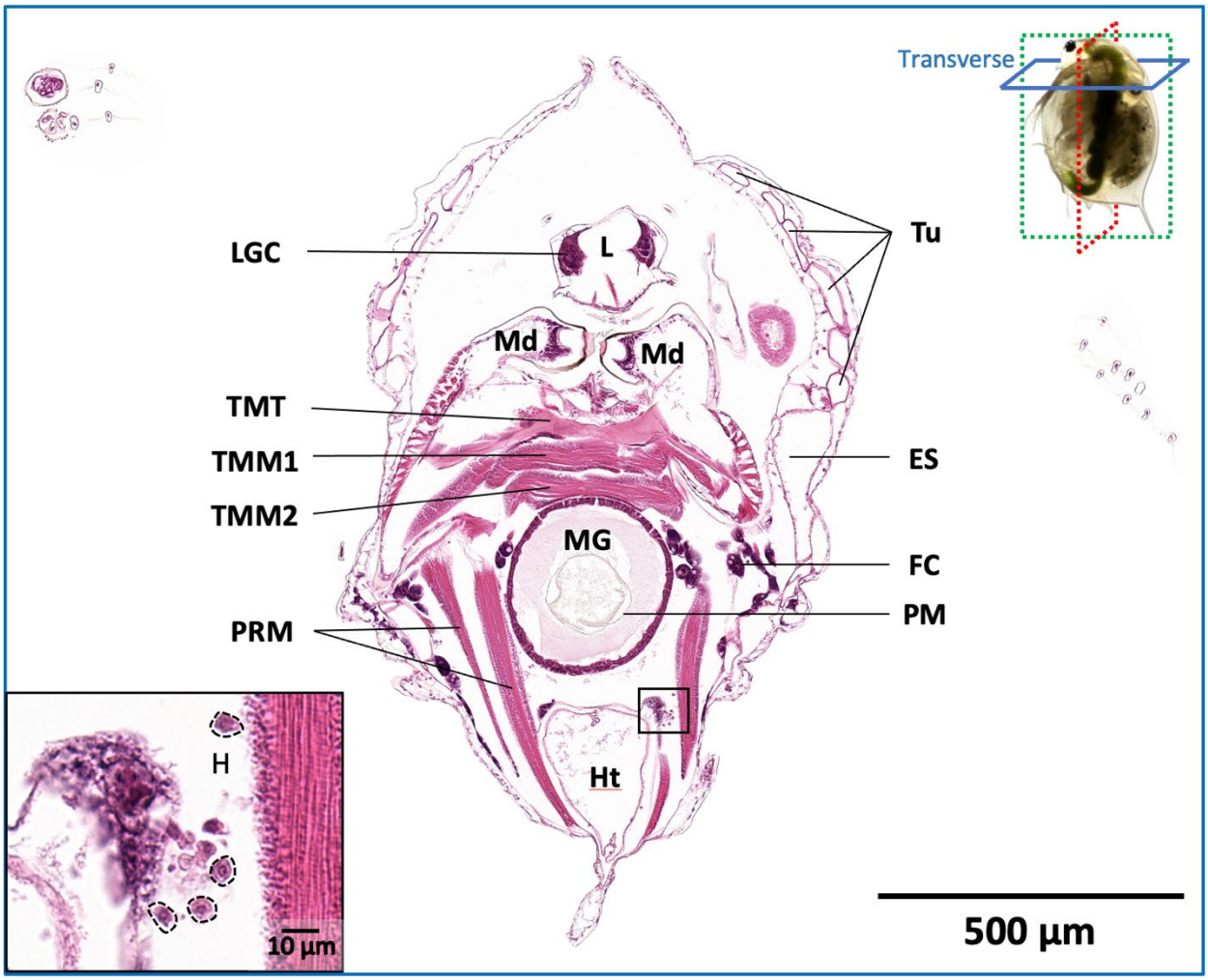

Figure 6. Representative image showing anatomical structures of female *D. magna* in the transverse plane. The transverse plane shows the asymmetrical paired mandibles (Md) with the transverse mandibular tendons (TMT), transverse mandibular muscles (TMM1), transverse muscles of mandibles (TMM2), and the posterior rotator muscles of mandibles (PRM). Other features seen include labrum (L) that houses labral gland cells (LGC), end sac (ES) and tubules (Tu) of the maxillary gland, midgut (MG) with the peritrophic membrane (PM), and the heart (Ht). Inset displays several hemocytes (H) outlined by dotted circles.
Corresponding atlas link: http://daphnia.io/anatomy/histology/?t=transverse_female&z=10

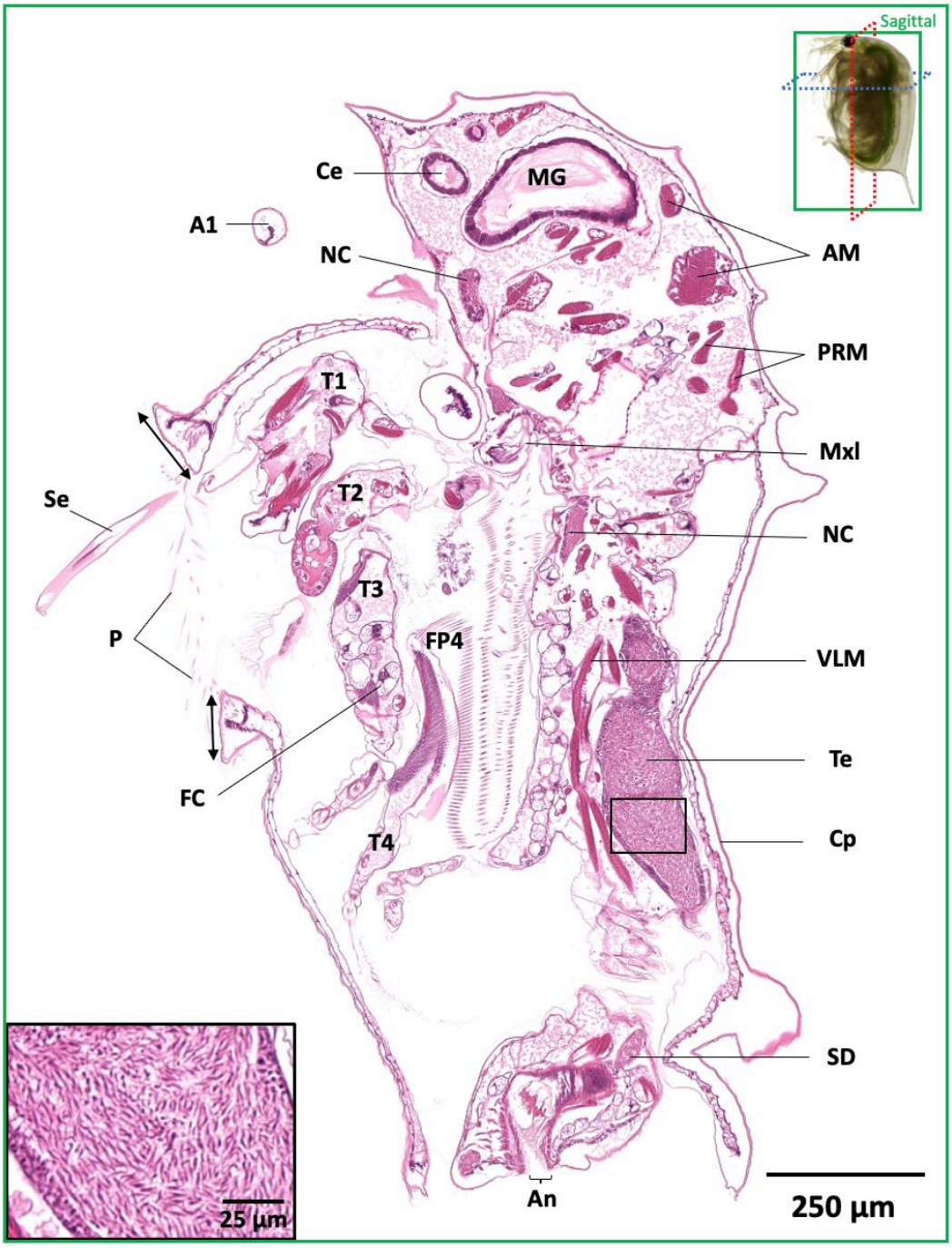

Figure 7. Representative image showing anatomical structures of male *D. magna* in the sagittal plane. The sagittal plane shows the elongated seta (Se) on the first thoracic limb, pubescence (P) at the wider ventral opening of carapace, thickening of carapace at the ventral opening (arrows), one of the testes (Te), and a small portion of sperm duct (SD). Inset showing the spermatozoa in the testis. A1, antennule; A2M, antennal muscle; An, anus; Ce, hepatic cecum; Cp, carapace; ES, end sac of the maxillary gland; FC, fat cell; FP4, filter plate 4; Ht, heart; L, labrum; Md, mandible; MG, midgut; Mxl, maxillule; NC, nerve cord; PRM, posterior rotator muscle of mandible, T1-4, thoracic appendage 1-4; VLM, ventral longitudinal muscle. Corresponding atlas link: http://daphnia.io/anatomy/histology/?t=sagittal_male&z=3

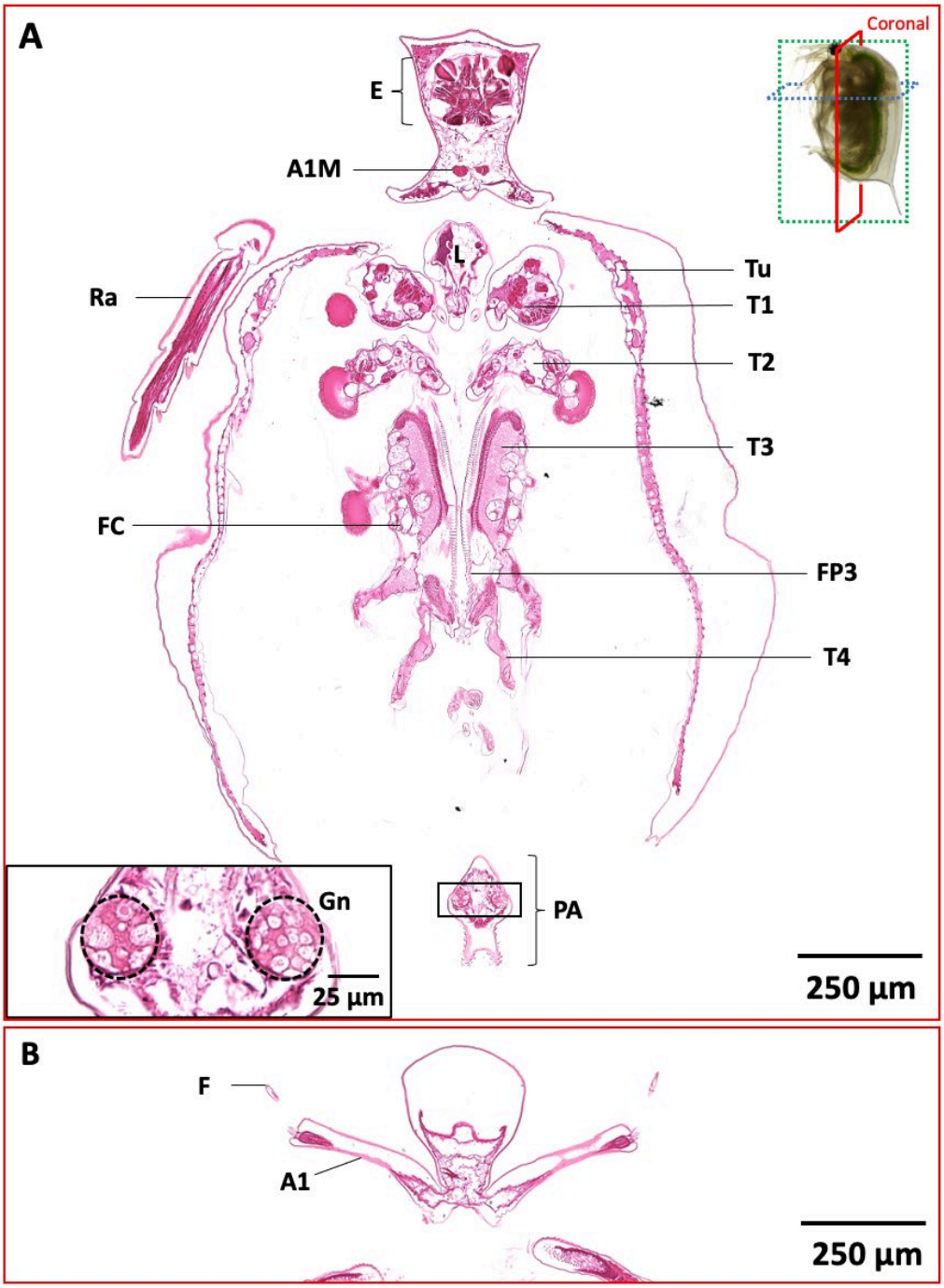

Figure 8. Representative images showing anatomical structures of male *D. magna* in the coronal plane. (A) This coronal section shows the antennule muscles (A1M) that are only present in the male, the first four paired thoracic limbs (T1-T4), and the gonopores (Gn, dotted circles in inset) on the postabdomen (PA). **(B)** This section, slightly ventral to panel A, displays the prominent and elongated antennules (A1) with flagella (F) at the tip. E, compound eye; FC, fat cell; FP3, filter plate 3; L, labrum; Ra, ramus of swimming antenna; Tu, tubule of the maxillary gland. Corresponding atlas links:
(A) https://daphnia.io/anatomy/histology/?t=coronal_male&z=4
(B) http://daphnia.io/anatomy/histology/?t=coronal_male&z=2&c=0.2,0.14,0.6,0.4

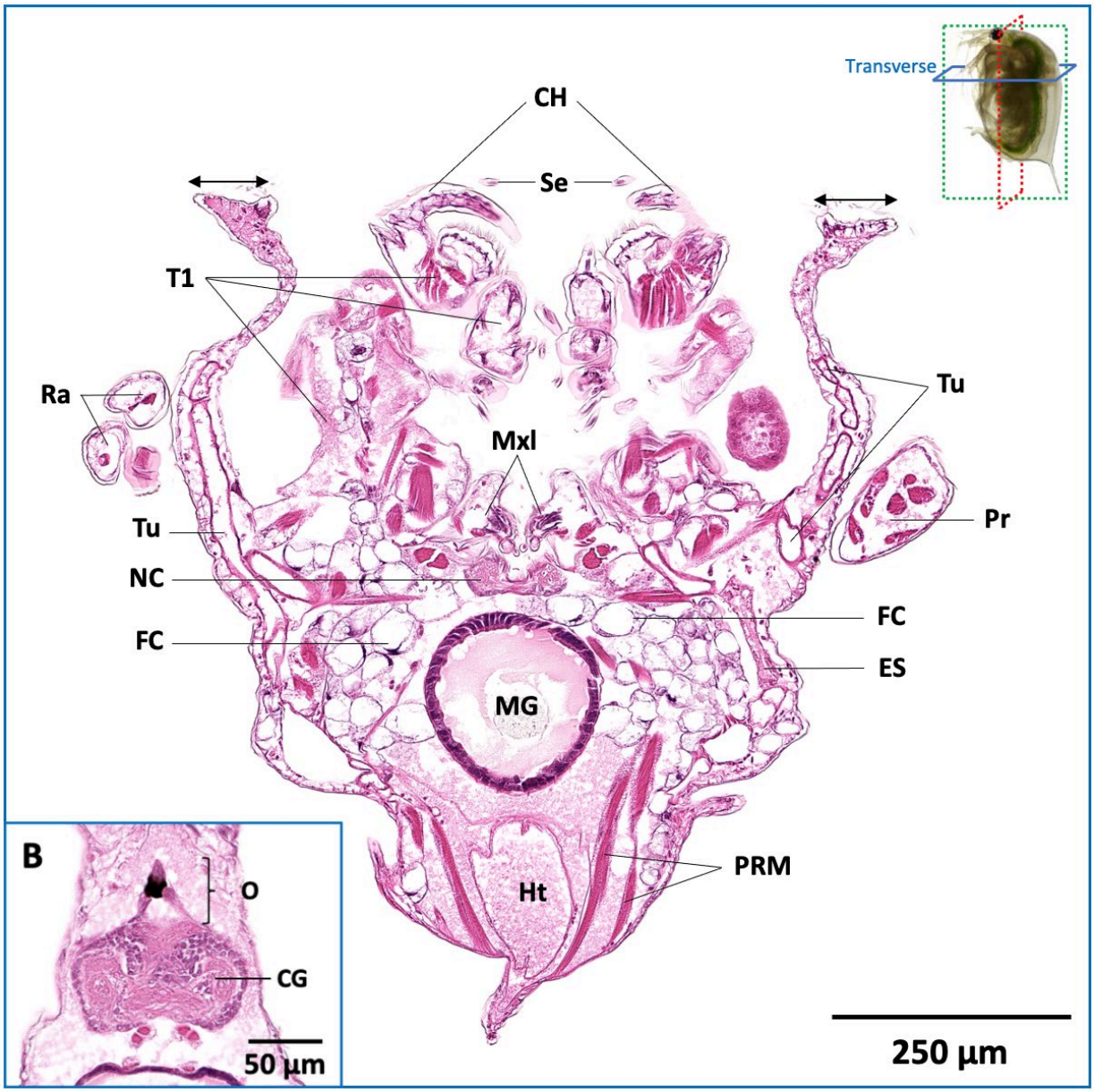

Figure 9. Representative image showing anatomical structures of male *D. magna* in the transverse plane. (A) This transverse section displays the paired copulatory hooks (CH) and elongated setae (Se) on the first thoracic limbs (T1), with pubescence and thickening of the carapace (arrows) at the ventral opening. This also shows the abundance of fat cells (FC) around the midgut (MG). Cp, carapace, ES, end sac of the maxillary gland; Ht, heart; L, labrum; Mxl, maxillule; NC, nerve cord; PRM, posterior rotator muscle of mandible; Pr, protopodite of swimming antenna; Ra, ramus of swimming antenna; Tu, tubule of the maxillary gland. **(B)** Pigmented ocellus (O) is shown connected to the cerebral ganglion (CG). This transverse section is slightly above that of panel A.

Corresponding atlas links:

(A) https://daphnia.io/anatomy/histology/?t=transverse_male&z=8

(B) http://daphnia.io/anatomy/histology/?t=transverse_male&z=4&c=0.43,0.25,0.18,0.12

242 Circulatory system

243 *Daphnia* have an open circulatory system and a myogenic heart (Stein et al., 1966; Steinsland,
244 1982). The heart (Ht) has a pair of ostia situated immediately to the anterior of the brood chamber,
245 between the midgut and dorsal surface (Figures 4, 6, 8). As *Daphnia* are semi-transparent, the
246 beating heart and the flow of hemolymph (blood) containing hemocytes (H) or blood cells (Figure
247 6 inset) can be easily observed (Auld et al., 2010; Metschnikoff, 1884) under low magnification.
248

249 Digestive system

250 *Daphnia* are filter feeders. Food particles are filtered through filter plates (FP3 and FP4) consisting
251 of setae on thoracic limbs 3 and 4, passed through maxillules (Mxl) and mandibles (Md) to enter
252 the esophagus (Eso), which is the first part of the digestive system (Figures 4). The digestive
253 system also consists of paired hepatic ceca (Ce), midgut (MG), and hindgut (HG) (Figures 4, 5, 6,
254 7, and 9) that are lined with epithelial cells and microvilli, with the columnar epithelial cells in the
255 midgut and cuboidal cells in hepatic ceca and hindgut (Quaglia et al., 1976; Schultz and Kennedy,
256 1976). The labrum (L) houses labral gland cells (LGC) that have been suggested to be involved in
257 food ingestion and endocrine function (Zaffagnini and Zeni, 1987; Zeni and Franchini, 1990)
258 (Figures 4, 6, and 8).
259

260 Excretory system

261 The maxillary gland, also known as the shell gland, is the organ of excretion of *Daphnia,* housed
262 between the inner and outer walls of the carapace. It consists of an end sac (ES), a series of tubules
263 (Tu), and an opening to the outside that is situated within the anterior part of the brood chamber
264 (Smirnov, 2017) (Figures 5, 6, 8A, and 9A).
265

266 Locomotive and osmotic regulation

267 The second pair of antennae also referred to as swimming antennae, is the primary organ of
268 locomotion. Each swimming antenna has a protopodite (Pr), two rami (Ra) bearing setae (Se)
269 (Agar, 1950) (Figure 5, 8A, 9A), and is supported by antennal muscles (A2M). *Daphnia* has five
270 thoracic limbs (T1-T5) (Benzie, 2005) (Figures 4, 7, and 8A). Movements of thoracic limbs
271 produce a constant current that brings food particles into the digestive tract (Bednarska, 2006;
272 Fryer, 1991) and facilitates osmotic regulation, which occurs in the epipodite on each thoracic limb

273 (Kikuchi, 1983). First thoracic limbs in male *Daphnia*, having elongated setae (Figure 7) and
274 copulatory hooks (Figure 9), are different from those in the female.
275
276 Muscular system
277 The muscular system is very prominent and occupies a significant portion of the body. The largest
278 muscles are ventral and dorsal longitudinal muscles (VLM and DLM) that extend along the gut,
279 three paired antennal muscles (A2M), transverse mandibular muscles (TMM1), transverse muscles
280 of mandibles (TMM2), posterior rotator of the mandibles (PRM), carapace adductor muscles
281 (ACAM and PCAM) (Figures 4, 5, 6 and 7), and followed by groups of muscles that allow the
282 motion of thoracic limbs and postabdomen (Binder, 1931; Fryer, 1991). Other small muscles
283 include those around the compound eye (Binder, 1931; Consi et al., 1987), labrum (Binder, 1931),
284 and esophagus (Binder, 1931). All muscles are striated and surrounded by sarcoplasm, which
285 contains many nuclei and is mostly vacuolated. Sarcoplasm is particularly abundant and more
286 vacuolated in the antennal muscles.
287
288 Nervous, sensory, and vision system
289 *Daphnia magna* have a pigmented compound eye (E) consisting of 22 ommatidia, derived from
290 two eyes that fuse during embryonic development, and a small, pigmented ocellus (O) with three
291 lens-like bodies (Figure 9B). The optic nerve (ON) of each ommatidium forms a parallel bundle
292 that connects to the optic lobe of cerebral ganglion (OL), which is then connected to the cerebral
293 ganglion (CG) (Figure 4). The cerebral ganglion is connected to two chains of nerve cords (NC)
294 that run along the thorax (Figures 5, 7 and 9), underneath the gut, and reach other anatomical
295 structures (Kress et al., 2016; McCoole et al., 2011; Weiss et al., 2012).
296
297 Reproductive system
298 The ovaries in females (Figure 5) and the testes in males (Figure 7) are paired and situated ventrally
299 along the gut. *Daphnia* and all other species of the order Cladocera are cyclical parthenogens,
300 which involves both sexual (meiotic) and clonal (ameiotic) reproduction (Decaestecker et al.,
301 2009). Under favorable environmental conditions, females reproduce parthenogenetically, and
302 broods of genetically identical embryos will develop in the brood chamber before being released.
303 Sexual reproduction is cued by environmental stress (often seasonal, including photoperiod,

304 temperature, and over-crowding) that triggers the production of genetically identical males instead
305 of females. During this sexual phase of the *Daphnia* life cycle, females also switch to producing
306 two haploid eggs. Unlike parthenogenetic embryos, the development of these sexually produced
307 embryos is arrested at the 3000 cell stage (Chen et al., 2018) and enter into a state of dormancy
308 while being encased within an ephippium that protects these embryos under diapause through
309 harsh environmental conditions for decades and even centuries (Cáceres, 1998; Mergeay et al.,
310 2004). These two 'resting eggs' are different from parthenogenetically produced eggs that can
311 number up to 100 per brood. Parthenogenetic eggs contain multiple oil droplets (od) of varying
312 size and yolk granules (yg) that are generally larger in size (Hiruta and Tochinai, 2014) (Figure
313 10).
314
315 Testes of male *Daphnia* consist of two long tubular structures that are connected to gonopores
316 (Gn) or ejaculatory openings by sperm ducts (Figure 7). Spermatogenesis begins at the testes'
317 walls, and mature spermatozoa are displaced inward toward the central region of the testes (Wuerz
318 et al., 2017).
319
320 Fat cells, which are polyploid (Beaton and Hebert, 1989), consist of a massive portion of lipid and
321 glycogen (Zaffagnini and Zeni, 1986), are abundant in healthy *Daphnia*. They are found along the
322 gut, on the thoracic limbs, and around ovaries or testes (Figure 4, 5, 6, 7, 8A, and 9A). These cells
323 are most likely sites of the vitellogenin synthesis (Zaffagnini and Zeni, 1986) and have been
324 implicated with epipodite cells (on thoracic limbs) in the synthesis of hemoglobin (Goldmann et
325 al., 1999).
326

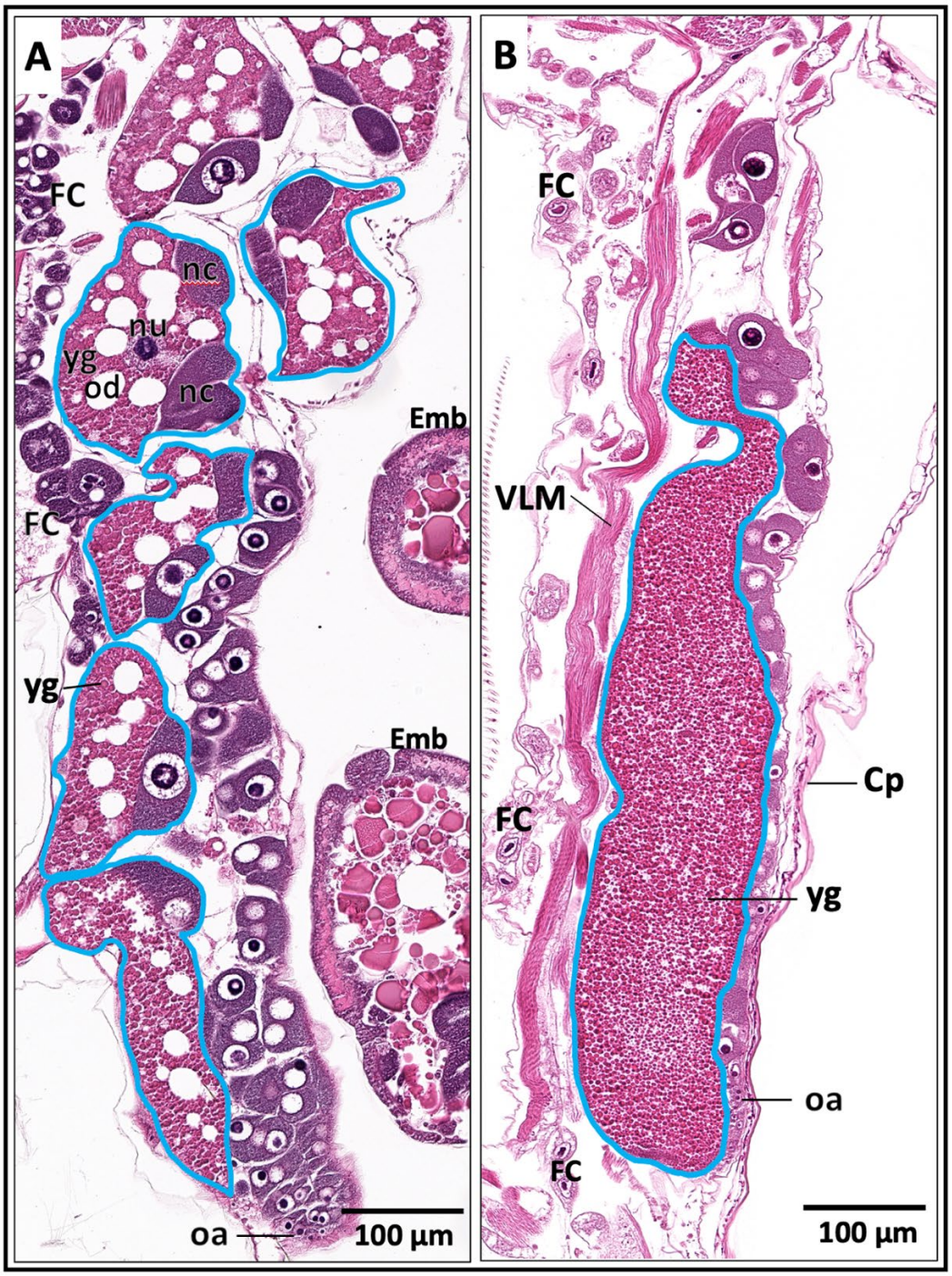

Figure 10. Comparison of ovarian eggs in females reproducing parthenogenetically or sexually. (A) The ovarian eggs of a female reproducing parthenogenetically contain a large amount of oil droplets (od) and yolk granules (yg) that are generally larger in size. **(B)** The ovarian egg of a female reproducing sexually contains a large proportion of fine yolk granules without oil droplets. Cp, carapace; Emb, embryo; FC, fat cell; nc, nurse cell; nu, nucleus of oocyte; Oa, oogonia; VLM, ventral longitudinal muscle. A solid blue circle indicates an individual ovarian egg.

336 2.4.1 Sexual dimorphism in *Daphnia*

337 Sexual dimorphism in *Daphnia* includes smaller male body size and male prominence and
338 elongation of antennules (A1), uniquely with flagella (F) at their tips (Figure 8B). Male antennules
339 carry muscles (A1M) (Figure 8A) that are absent in the females. Males also have a wider opening
340 and thickening of integument at the ventral margin of the carapace (Figures 7, 9A, and 11) which
341 is covered by pubescence (P) or fine hairs (Figures 7 and 9). The first thoracic limbs of the males
342 are equipped with elongated setae (Figure 7) and chitinized copulatory hooks (Figure 9) that are
343 used for clasping females during copulation. The male postabdomen has only one abdominal
344 process but has gonopores (Figure 8A inset) that are involved in transferring mature spermatozoa
345 from testes to the female in the region of the oviduct during copulation. Fat cells in both sexes go
346 through periodical changes but fat cells in the males are different from those in females as they
347 generally contain much larger lipid droplets, reduced and less granular cytoplasm, and smaller
348 nucleoli that are usually situated at the cell periphery (Figure 12).

349

350 *Doublesex* genes *(Dsx1)* in *D. magna* had been reported to exhibit sexual dimorphic differences in
351 the abundance of its transcripts that were primarily detected in the male-specific structures (Kato
352 et al., 2011; Nong et al., 2017). Time-lapse imaging showed that with the exception of elongated
353 antennules and the gonad, most male-specific structures start developing at instar 5 (7-day post-
354 ovulation) (Nong et al., 2017) during the early juvenile stage. The male-specific expression had
355 been detected in other anatomical structures, such as compound eye (Kato et al., 2011) and skeletal
356 muscles (Nong et al., 2017), of which sex difference has not been reported to date. It is envisioned
357 that spatially-resolved -omics studies assisted by histology images will add insight into the roles
358 of gene regulation, proteins, and other molecules in physiological function in the morphogenesis
359 of sexual dimorphism in *Daphnia*.

360

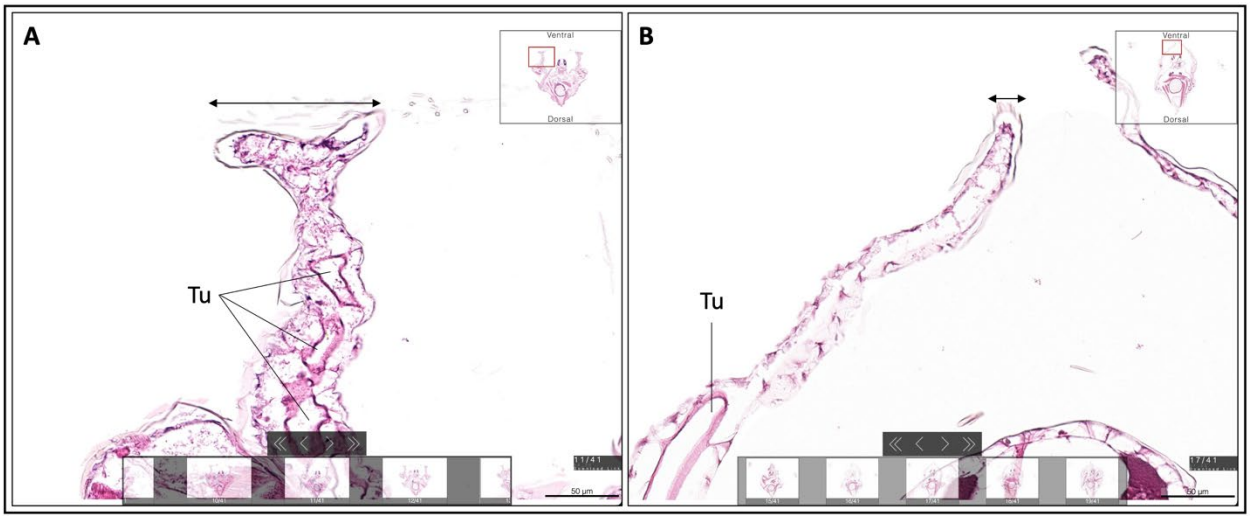

Figure 11. Comparison of male and female carapace at the ventral opening. (A) Thickening of the male carapace (arrow) at the ventral opening is shown as compared to that of the **(B)** female. Tu, Tubules of the maxillary gland. Corresponding atlas links:
(A) http://daphnia.io/anatomy/histology/?t=transverse_male_88&z=11&c=0.23,0.105,0.23,0.18
(B) http://daphnia.io/anatomy/histology/?t=transverse_female_57&z=17&c=0.36,0.07,0.20,0.15

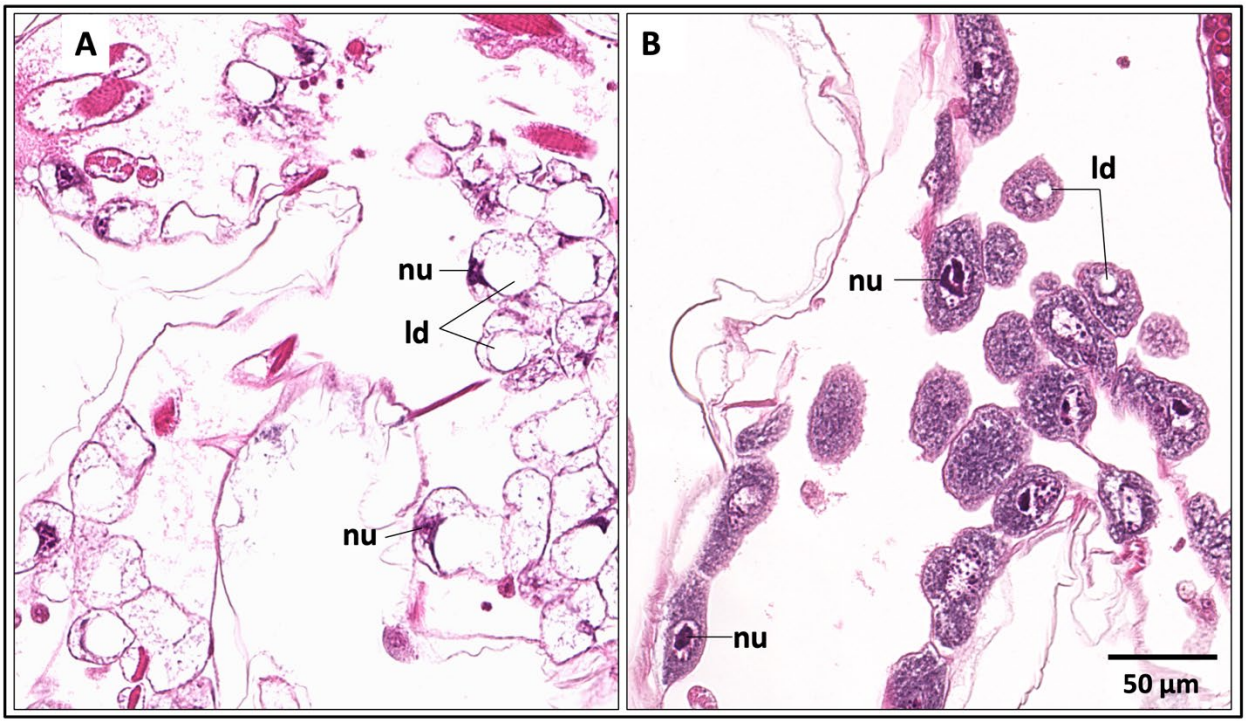

Figure 12. Comparison of male and female fat cells. (A) Fat cells in the male consist of larger lipid droplets (ld), reduced and less granular cytoplasm with smaller nucleoli (nu) that are situated at the cell periphery. **(B)** Fat cells in the female have more granular cytoplasm with smaller lipid droplets (ld) and bigger nucleoli (nu). Corresponding atlas links:
(A) http://daphnia.io/anatomy/histology/?t=sagittal_male&z=2&c=0.34,0.48,0.29,0.19
(B) http://daphnia.io/anatomy/histology/?t=sagittal_female&z=7&c=0.38,0.75,0.21,0.14

376 *2.5 Future Prospects and Applications*

377 Atlases are foundational to the systematic characterization of anatomical (i.e., cellular and tissue)
378 structures of organisms in both healthy and diseased states. An essential step towards the
379 identification of adverse conditions and outcomes is the documentation of healthy and normal
380 structures in adults. The *Daphnia* histology reference atlas presented here was created in
381 recognition of *Daphnia* as a model organism for biology, especially toxicology and ecotoxicology
382 that now includes extensive environmental genomics and metabolomics (Kim et al., 2015; Shaw
383 et al., 2008; Tkaczyk et al., 2021) but currently lacks correlation with microanatomical
384 (histopathological) phenotypes. This reference atlas provides the histological component of
385 anatomical context for both sexes of *D. magna,* using a web-based interface that is far more
386 accessible to the average user than traditional paper-based atlases. With this atlas as a foundation
387 for whole-organism evaluation, histopathological changes detected within a whole organism can
388 be correlated with toxicological -omics data that require spatial context to understand and to allow
389 a more comprehensive understanding of toxicological effects across cell types, organ systems, and
390 organisms. This integration of data is critical for discovering and applying adverse outcome
391 pathways (OECD, 2022) for next-generation risk assessment (US EPA, 2014) where there is no
392 predetermined link between biomarkers of adversity, causative agents, and organ-specific effects.
393 This will help to draw cause-effect relationships between environmental toxicants, tissue-specific
394 adverse effects in sentinel and test organisms, and human and animal disease associated with
395 environmental toxicants. The addition of pathological effects to the atlas will facilitate and make
396 histological data more actionable in terms of hazard and/or risk assessment and regulatory
397 decision-making for environmental health protection.

398

399 This atlas is envisioned to serve as a potential integrative platform for other omics data and to
400 facilitate the addition of context from other imaging modalities. Notably, adding microanatomical
401 context to molecular analyses including transcriptomics (Marx, 2021), secondary ion mass
402 spectrometry (Bonnin and Rizzoli, 2020), and desorption electrospray ionization-mass
403 spectrometry (Smith et al., 2022), has become a new priority, and typically relies on tissue
404 histology to which the data can be mapped. While 3D imaging modalities such as fluorescence-
405 based confocal or laser sheet microscopy (Connelly et al., 2015; Mittmann et al., 2014), or X-ray
406 histotomography (Ding et al., 2019; Yakovlev et al., 2022) provide the 3-dimensionality of

407 anatomical structures that is lacking in histology, differential staining using a range of
408 histochemical stains provides the basic understanding of tissue and cell types that can eventually
409 be linked to the grayscale morphologies characteristic of most 3D imaging modalities. Cross-
410 referencing between 2D and 3D imaging modalities such as that illustrated in Figure 13 would
411 serve to increase the value of each and enhance the utilization. Note that the understanding of
412 structures in 3D images from any imaging mode requires inspection of 2D images, including 2D
413 slices and 3D renderings, both of which can benefit from the atlas labeling and visualization tools
414 (Figure 13C). Work is underway to add 3D data into the histology atlas, including multiple whole
415 *D. magna* X-ray histotomograms. Quantitative analysis based on automated segmentation of
416 cellular and tissue components, if developed, would comprise an important foundation for the
417 development of toxicological phenomics across model systems.
418
419 Whole organism atlases are crucial for the elucidation of the anatomical and functional
420 organization of tissues and organs. They are also essential as an integrative spatial framework for
421 examining and identifying morphological and cellular change. The significant effort and resources
422 required of adding toxicological data to the web-based whole-organism atlas will be outweighed
423 by its essential role in ensuring quality, validation, and reproducibility of toxicological research,
424 and facilitating education, data sharing, and collaboration. The foundation for whole-organism
425 atlas is a representative set of high-resolution digital slides (at least 40X magnification)
426 encompassing a whole organism. The web-based platform allows the visualization of high-
427 resolution digital slides without requiring local file storage or downloading. Our platform also
428 enables the interactive presentation of color-coded annotation of anatomical structures. The
429 pipeline of *Daphnia* histology reference atlas (Figure 14) was created with the intent to extend its
430 features for the benefit of the research that uses other model or sentinel organisms and would be
431 particularly exciting for cross-phylogenetic atlases and for global collaborative projects such as
432 the Encyclopedia of Life (Parr et al., 2014).
433

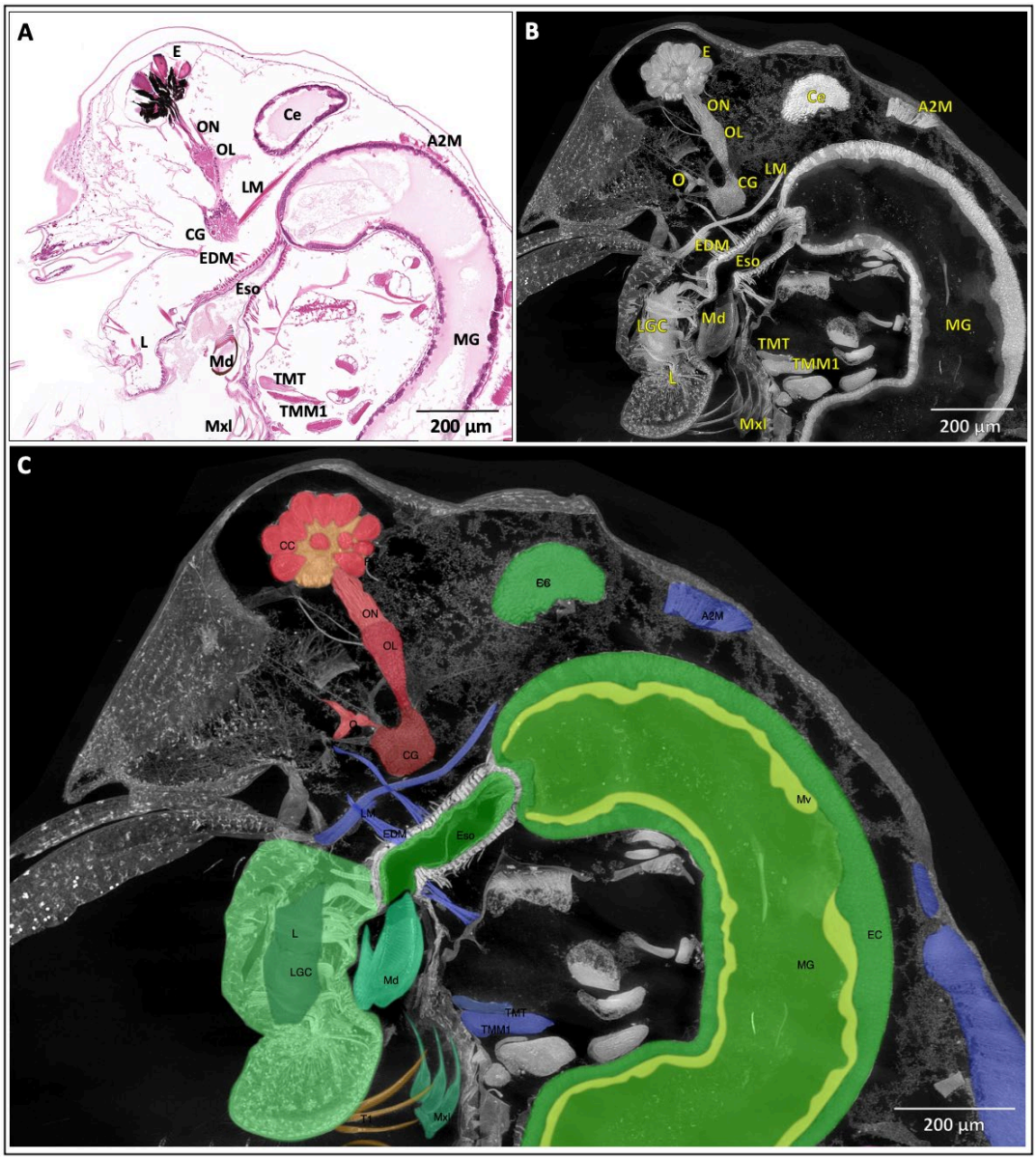

Figure 13. Cross-referencing of histology with microCT-based X-ray histotomography. (A) The anatomical structures of a female *D. magna* in a 5 µm histology section, cross-referenced to **(B)** a 25 µm stack from a histotomographic reconstruction of another female *D. magna* that provides more spatial context of various anatomical structures via easily adjustable stack thickness. Note that the connection of ocellus (O) to the cerebral ganglion (CG) and the 3-dimensionality of the compound eye (E) are demonstrated by the 25 µm histotomographic stack in panel B. **(C)** Color-overlay highlighting of the 25 µm stack shown in panel B, available in the atlas at http://daphnia.io/anatomy/histotomography/?t=AAA392&z=1&c=0.18,0.02,0.79,0.55. A2M, antennal muscle; Ce, hepatic cecum; CC, crystalline cone of ommatidium, EC, epithelial cell of midgut; EDM, esophageal dilator muscle; Eso, esophagus; L, labrum; LGC, labral gland cell; LM, levator muscle of labrum; Md, mandible; Mv, microvilli of midgut; Mxl, maxillule; MG, midgut; OL, optic lobe of cerebral ganglion; ON, optic nerve; TMM1, transverse mandibular muscle; TMT, transverse mandibular tendon.

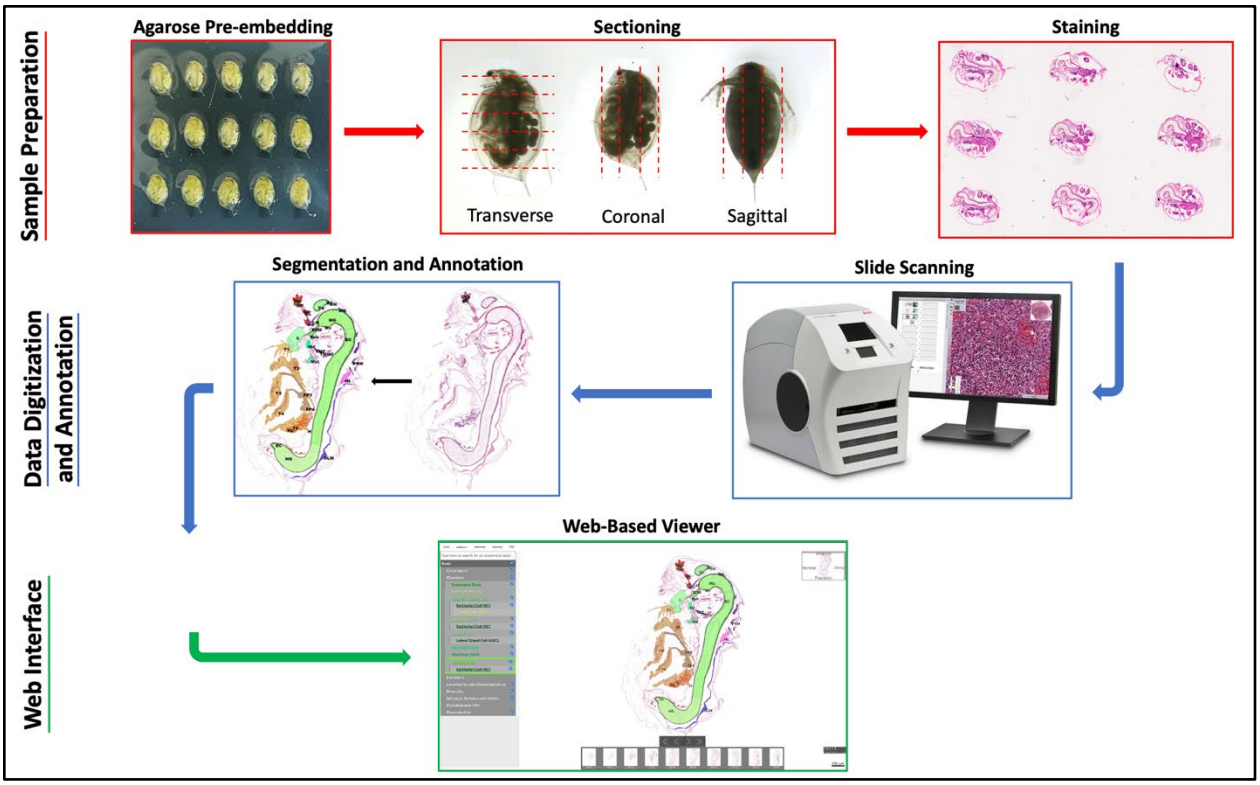

Figure 14. Overview of the creation of *Daphnia* histology reference atlas.

3. Material and Methods

3.1 *Daphnia magna* husbandry

Daphnia magna were purchased from Carolina Biological (NC, USA) and raised in "Aachener Daphnien-Medium" or ADaM (Klüttgen et al., 1994) with modified content of selenium at room temperature (20°C ± 1°C) under a 16-hour light/8-hour dark photoperiod. *Daphnia magna* were fed three times weekly with 3.0 x 10^7 cells/ml of green microalgae (*Raphidocelis subcapitata)* and 0.1 mg/mL of dissolved bakers' yeast. The animal density was maintained at about 20 neonates, 10 juveniles and 5 to 7 reproducing adults per liter to prevent overcrowding and trigger the production of resting eggs and male *D. magna*. Under these conditions, animals reached maturity 6 to 8 days post-birth and reproduced parthenogenetically every 3 days with an average of 15 neonates per brood from the second brood onwards. Production of males and females carrying resting eggs was induced by overcrowding (>10 reproducing adults per liter) and shorter photoperiod (10 h).

3.2 Fixation and decalcification

466 *Daphnia magna* were euthanized in glass vials filled with bicarbonate water. Live *D. magna* were
467 transferred using plastic transfer pipettes. Tips of transfer pipettes were trimmed at a 45° angle
468 such that the diameter was double the size of the samples. Immediately following euthanasia,
469 bicarbonate water was gently removed with a transfer pipette and replaced with at least 20X
470 specimen volume of Bouin's solution (Newcomer Supply, WI) for fixation. The *D. magna* samples
471 were immersed in fixative on a low-speed orbital shaker (Corning LSE) set to 55 revolutions per
472 minute (RPM). We tested several fixatives and fixation parameters, such as duration and
473 temperature listed in Table 1. After fixation in Bouin's solution, samples were washed twice using
474 1X phosphate-buffered saline (PBS) for 10 min each time. This was followed by decalcification
475 in 20X sample volume of cold 6% formic acid (Sigma-Aldrich, MO) for 24 hours. Samples were
476 then rinsed in 70% ethanol for one minute and immersed in fresh 70% ethanol for 30 min before
477 agarose pre-embedding.
478
479 Table 1: Fixation parameters

Fixative	Fixation time and temperature	Decalcification by cold 6% formic acid time and temperature
Bouin's solution	48 h, 4 °C	24 h, 21 °C
	48 h, 21 °C	24 h, 21 °C
4% Paraformaldehyde	48 h, 4 °C	24 h, 4 °C
	48 h, 21 °C	24 h, 4 °C
10% Neutral buffered formalin	48 h, 4 °C	24 h, 4 °C
	48 h, 21 °C	24 h, 4 °C

480
481 3.3 Mold and agarose embedding
482 Samples were pre-embedded in 1% agarose block casted using "triangle mold" (Figure 1A-B) for
483 histological processing following a protocol adapted from Sabaliauskas et al. (2006). After taping
484 around the triangle mold, 2.5 mL of 1% agarose (Sigma-Aldrich, MO) at 55 °C were pipetted onto
485 the mold, and then let solidify at room temperature (Figure 1C). Once solidified, the agarose block
486 was removed gently from the mold (Figure 1D). Then, *D. magna* samples were transferred onto
487 the agarose block using a plastic pipette. A thin layer of 70% ethanol was pipetted onto the block
488 to help with the positioning of samples. Samples designated for the sagittal plane were laid on their
489 sides with a swimming antenna in the wells and all rostra facing the same direction. Samples
490 designated for coronal and transverse orientation were laid on their back in the wells (Figure 1 E-

F). Once all the samples were positioned in individual wells, excess ethanol was carefully dried off using lint-free Kimwipes without agitating the samples. Each sample was first topped-off with one drop of molten 1% agarose (about 50 °C) without moving the sample, followed by a thin layer of 1% agarose covering all the samples. After the agarose solidified (~ 5 minutes at room temperature), the block was trimmed, placed into a tissue cassette, and stored in 70% ethanol for tissue processing. During paraffin embedding, the agarose blocks were positioned in the appropriate final orientation (transverse, sagittal or coronal) for sectioning.

3.4 Processing, sectioning, and staining

All samples were dehydrated and infiltrated in RMC Model 1530 automated closed reagent type tissue processor (Table 2). The *D. magna* samples were serially sectioned at 5 µm on a Leica RM2255 automated rotary microtome. Sections were then stained with Harris' hematoxylin and eosin (H&E) in an auto-stainer (Sakura Tissue Tek DRS 2000, IMEB, CA) following protocol adapted from Copper et al. (2018). The duration of hematoxylin staining was extended from 3 to 7 min to achieve better contrast for samples fixed with Bouin's solution (Table 3).

Table 2: Tissue Processing Steps

Duration	Solution	Temp (°C)	Vacuum (in. Hg)
45 min	80% Ethanol	25	15
45 min	95% Ethanol	25	15
1 hour	95% Ethanol	25	15
1 hour (repeat thrice)	100% Ethanol	25	15
1 hour (repeat twice)	Xylene	25	15
1 hour 30 min (repeat twice)	Paraffin	60	15
2 hours	Paraffin	60	15

516 Table 3: Automated staining steps

Time	Solution
3 min	Xylene
5 min	Xylene
2 min (repeat twice)	100% Ethanol
2 min	95% Ethanol
10 min	Tap water
7 min	Hematoxylin
1 min	Tap water
1 min	Acidified Alcohol
1 min	Tap water
0.2 min	Ammoniated water
1 min	Tap water
0.3 min	Eosin
1 min	30% Ethanol
1 min	95% Ethanol
1 min	100% Ethanol
1 min	Xylene

517

518 3.5 Histology slide digitization

519 All slides were scanned using an Aperio AT2 slide scanner (LeicaBiosystems, IL) and saved in
520 TIFF format as digital slides. The regions of selected *D. magna* samples were then extracted using
521 Image Scope. Three channels (Red, Green, Blue) of these digital slides were stacked using Fiji,
522 oriented, and post-processed for background removal using Adobe Photoshop. Each set of digital
523 slides was then pyramidally tiled (libvips) in preparation for the web-based viewer.

524

525 3.6 Labeling and segmentation workflow

526 For each anatomical structure included in the anatomical ontology (a list of terms organized by
527 groups and subgroups, Supplemental File 3), we began by reviewing published literature, then
528 concluding with a visual analysis of the structure in each of the three orthogonally cut histology
529 slide sets. Anatomical structures included in the anatomical ontology were grouped and color-
530 coded based on organ systems. Labeling and segmentation of anatomical structures were done one
531 image at a time in Adobe Illustrator. The Adobe Illustrator Layer of an anatomical structure was
532 first labeled corresponding to the appropriate ontological term. Each anatomical structure was
533 segmented by outlining the structure with the curvature tool. Segmentation was then assigned the

color based on the pre-determined color code. After completion of the labeling and segmentation of all anatomical structures on a given image, a single scalable vector graphic (SVG) was exported to be used as input for the web-based viewer.

3.7 Web-interface workflow

The file sizes associated with digital slides are on the order of >2 GB per slide, making scans challenging to view for users with standard computational resources. For easier access and usage of the data without the need to download full-resolution images, we developed an open-access, web-based digital slide viewing platform based on the open-access project OpenSeadragon (OpenSeadragon"). This viewer combines annotations and digital scans into a seamless experience to provide user-friendly access to high-resolution data. The atlas' code was written in client-side JavaScript, HTML, and CSS requires no traditional download and has no server requirement to run the basic implementation. Pyramidally tiled images are parsed and visualized with OpenSeadragon. When the user loads a new image, the viewer opens the corresponding SVG file. The SVG file contains all the anatomical labels on a given image and their corresponding shape vector information. The viewer parses all labels from the <g> element of the SVG file, plotting the corresponding regions on the viewer itself, and updates the ontology to note what regions are available to visualize on the current image.

Acknowledgments

The authors want to acknowledge Penn State Human Health and Environment Seed Grant supported by Pennsylvania Department of Health Commonwealth Universal Research Enhancement Program Grant. The Department of Health specifically disclaims responsibility for any analyses, interpretations, or conclusions. The authors also acknowledge NIH grant 1R24OD18559 to KCC and Jake Gittlen Laboratories for Cancer Research. The authors are grateful to Patrick Leibich and the Department of Surgery, Penn State College of Medicine for 3D-SLA printing the casting molds. The authors also want to thank Chadwick Harris and Debra Shearer for helping with histology sectioning and slide staining. This work contributes to the PrecisionTox project that has received funding from the European Union's Horizon 2020 research and innovation program under grant agreement No 965406.

Competing Interests

The authors declare no competing interest.

References

Agar WE. 1950. The swimming setae of *Daphnia carinata*. *J Cell Sci* **s3-91**:353–368. doi:10.1242/jcs.s3-91.16.353

Au DWT. 2004. The application of histo-cytopathological biomarkers in marine pollution monitoring: a review. *Mar Pollut Bull* **48**:817–834. doi:10.1016/j.marpolbul.2004.02.032

Auld SKJR, Scholefield JA, Little TJ. 2010. Genetic variation in the cellular response of *Daphnia magna* (Crustacea: Cladocera) to its bacterial parasite. *Proc R Soc B Biol Sci* **277**:3291–3297. doi:10.1098/rspb.2010.0772

Beaton MJ, Hebert PDN. 1989. Miniature genomes and endopolyploidy in cladoceran crustaceans. *Genome* **32**:1048–1053. doi:10.1139/g89-552

Bednarska A. 2006. Adaptive changes in morphology of *Daphnia* filter appendages in response to food stress. *Polish Journal of Ecology* **54**:663–668.

Benzie JAH. 2005. The Genus *Daphnia* (including Daphniopsis) (Anomopoda:Daphniidae). Kenobi Productions.

Bernet D, Schmidt H, Meier W, Burkhardt-Holm P, Wahli T. 1999. Histopathology in fish: proposal for a protocol to assess aquatic pollution. *J Fish Dis* **22**:25–34. doi:https://doi.org/10.1046/j.1365-2761.1999.00134.x

Binder G. 1931. Das Muskelsystem von *Daphnia*. *Int Rev Gesamten Hydrobiol Hydrogr* **26**:54–98. doi:10.1002/iroh.19310260104

Bonnin EA, Rizzoli SO. 2020. Novel secondary ion mass spectrometry methods for the examination of metabolic effects at the cellular and subcellular levels. *Front Behav Neurosci* **14**:124. doi:10.3389/fnbeh.2020.00124

Cáceres CE. 1998. Interspecific variation in the abundance, production, and emergence of *Daphnia* diapausing eggs. *Ecology* **79**:1699–1710. doi:10.1890/0012-9658(1998)079[1699:IVITAP]2.0.CO;2

Chakraborty S, Ray M, Ray S. 2010. Toxicity of sodium arsenite in the gill of an economically important mollusc of India. *Fish Shellfish Immunol* **29**:136–148. doi:10.1016/j.fsi.2010.02.025

Chen L, Barnett RE, Horstmann M, Bamberger V, Heberle L, Krebs N, Colbourne JK, Gómez R, Weiss LC. 2018. Mitotic activity patterns and cytoskeletal changes throughout the progression of diapause developmental program in *Daphnia*. *BMC Cell Biol* **19**:30. doi:10.1186/s12860-018-0181-0

Christensen AK, Owusu NG, Jean-Louis D. 2018. Carapace epithelia are rich in large filamentous actin bundles in *Daphnia magna*, *Daphnia pulex*, and *Sida crystallina* (Crustacea: Cladocera). *Invertebr Biol* **137**:49–59. doi:10.1111/ivb.12204

Connelly SJ, Walling K, Wilbert SA, Catlin DM, Monaghan CE, Hlynchuk S, Meehl PG, Resch LN, Carrera JV, Bowles SM, Clark MD, Tan LT, Cody JA. 2015. UV-Stressed *Daphnia pulex* increase fitness through uptake of Vitamin D3. *PLOS ONE* **10**:e0131847. doi:10.1371/journal.pone.0131847

Consi TR, Macagno ER, Necles N. 1987. The oculomotor system of *Daphnia magna*. The eye muscles and their motor neurons. *Cell Tissue Res* **247**:515–523. doi:10.1007/BF00215744

609 Copper JE, Budgeon LR, Foutz CA, van Rossum DB, Vanselow DJ, Hubley MJ, Clark DP,
610 Mandrell DT, Cheng KC. 2018. Comparative analysis of fixation and embedding
611 techniques for optimized histological preparation of zebrafish. *Comp Biochem Physiol*
612 *Toxicol Pharmacol CBP* **208**:38–46. doi:10.1016/j.cbpc.2017.11.003
613 Decaestecker E, De Meester L, Mergeay J. 2009. Cyclical parthenogenesis in *Daphnia*: sexual
614 versus asexual reproduction In: Schön I, Martens K, Dijk P, editors. Lost Sex: The
615 Evolutionary Biology of Parthenogenesis. Dordrecht: Springer Netherlands. pp. 295–316.
616 doi:10.1007/978-90-481-2770-2_15
617 Ding Y, Vanselow DJ, Yakovlev MA, Katz SR, Lin AY, Clark DP, Vargas P, Xin X, Copper JE,
618 Canfield VA, Ang KC, Wang Y, Xiao X, De Carlo F, van Rossum DB, La Riviere P, Cheng
619 KC. 2019. Computational 3D histological phenotyping of whole zebrafish by X-ray
620 histotomography. *eLife* **8**:e44898. doi:10.7554/eLife.44898
621 Edwards C. 1980. The anatomy of *Daphnia* mandibles. *Trans Am Microsc Soc* **99**:2–24.
622 doi:10.2307/3226076
623 Environmental Protection Agency. 2002. Methods for measuring the acute toxicity of effluents
624 and receiving waters to freshwater and marine organisms.
625 Environmental Protection Agency. 1996. Ecological Effects Test Guidelines OCSPP850.1300:
626 Daphnid chronic toxicity test.
627 Fryer G. 1991. Functional morphology and the adaptive radiation of the Daphniidae
628 (Branchiopoda: Anomopoda). *Philos Trans R Soc Lond B Biol Sci* **331**:1–99.
629 doi:10.1098/rstb.1991.0001
630 Goldmann T, Becher B, Wiedorn KH, Pirow R, Deutschbein ME, Vollmer E, Paul RJ. 1999.
631 Epipodite and fat cells as sites of hemoglobin synthesis in the branchiopod crustacean
632 *Daphnia magna*. *Histochem Cell Biol* **112**:335–339. doi:10.1007/pl00007905
633 Halcrow K. 1976. The fine structure of the carapace integument of *Daphnia magna* Straus
634 (Crustacea Branchiopoda). *Cell Tissue Res* **169**:267–276. doi:10.1007/BF00214213
635 Haney JF, Hall DJ. 1973. Sugar-coated *Daphnia*: A preservation technique for Cladocera. *Limnol*
636 *Oceanogr* **18**:331–333. doi:https://doi.org/10.4319/lo.1973.18.2.0331
637 Hebert PDN, Ward RD. 1972. Inheritance during parthenogenesis in *Daphnia magna*. *Genetics*
638 **71**:639–642.
639 Hiruta C, Tochinai S. 2014. Formation and structure of the ephippium (resting egg case) in relation
640 to molting and egg laying in the water flea *Daphnia pulex* De Geer (Cladocera:
641 Daphniidae). *J Morphol* **275**:760–767. doi:10.1002/jmor.20255
642 Kato Y, Kobayashi K, Watanabe H, Iguchi T. 2011. Environmental sex determination in the
643 branchiopod crustacean *Daphnia magna*: Deep conservation of a Doublesex gene in the
644 sex-determining pathway. *PLoS Genet* **7**. doi:10.1371/journal.pgen.1001345
645 Kikuchi M, Sasaki Y, Wakabayashi M. 2000. Screening of organophosphate insecticide pollution
646 in water by using *Daphnia magna*. *Ecotoxicol Environ Saf* **47**:239–245.
647 doi:10.1006/eesa.2000.1958
648 Kikuchi S. 1983. The fine structure of the gill epithelium of a fresh-water flea, *Daphnia magna*
649 (Crustacea: Phyllopoda) and changes associated with acclimation to various salinities. I.
650 Normal fine structure. *Cell Tissue Res* **229**:253–268. doi:10.1007/BF00214974
651 Kim HJ, Koedrith P, Seo YR. 2015. Ecotoxicogenomic approaches for understanding molecular
652 mechanisms of environmental chemical toxicity using aquatic invertebrate, *Daphnia* model
653 organism. *Int J Mol Sci* **16**:12261–12287. doi:10.3390/ijms160612261

654 Klüttgen B, Dülmer U, Engels M, Ratte HT. 1994. ADaM, an artificial freshwater for the culture
655 of zooplankton. *Water Res* **28**:743–746. doi:10.1016/0043-1354(94)90157-0
656 Kress T, Harzsch S, Dircksen H. 2016. Neuroanatomy of the optic ganglia and central brain of the
657 water flea *Daphnia magna* (Crustacea, Cladocera). *Cell Tissue Res* **363**:649–677.
658 doi:10.1007/s00441-015-2279-4
659 Kühn R, Pattard M, Pernak K-D, Winter A. 1989. Results of the harmful effects of water pollutants
660 to *Daphnia magna* in the 21 day reproduction test. *Water Res* **23**:501–510.
661 doi:10.1016/0043-1354(89)90142-5
662 Kvist J, Athanàsio CG, Pfrender ME, Brown JB, Colbourne JK, Mirbahai L. 2020. A
663 comprehensive epigenomic analysis of phenotypically distinguishable, genetically
664 identical female and male *Daphnia pulex*. *BMC Genomics* **21**:17. doi:10.1186/s12864-019-
665 6415-5
666 LaDouceur EEB, Wynne J, Garner MM, Nyaoke A, Keel MK. 2016. Lesions of copper toxicosis
667 in captive marine invertebrates with comparisons to normal histology. *Vet Pathol* **53**:648–
668 658. doi:10.1177/0300985815603431
669 Lampert W. 2011. *Daphnia*: Development of a model organism in ecology and evolution, Book
670 21. ed, Excellence in Ecology. Oldendorf/Luhe: International Ecology Institute.
671 Marx V. 2021. Method of the Year: spatially resolved transcriptomics. *Nat Methods* **18**:9–14.
672 doi:10.1038/s41592-020-01033-y
673 McCoole MD, Baer KN, Christie AE. 2011. Histaminergic signaling in the central nervous system
674 of *Daphnia* and a role for it in the control of phototactic behavior. *J Exp Biol* **214**:1773–
675 1782. doi:10.1242/jeb.054486
676 Mergeay J, Verschuren D, Kerckhoven LV, Meester LD. 2004. Two hundred years of a diverse
677 *Daphnia* community in Lake Naivasha (Kenya): effects of natural and human-induced
678 environmental changes. *Freshw Biol* **49**:998–1013. doi:10.1111/j.1365-
679 2427.2004.01244.x
680 Metschnikoff E. 1884. A disease of *Daphnia* caused by a yeast. A contribution to the theory of
681 phagocytes as agents for attack on disease-causing organisms. *Archiv Pathol Anat Physiol*
682 *Klin Med* **96**:177–195.
683 Mittmann B, Ungerer P, Klann M, Stollewerk A, Wolff C. 2014. Development and staging of the
684 water flea *Daphnia magna* (Straus, 1820; Cladocera, Daphniidae) based on morphological
685 landmarks. *EvoDevo* **5**:12. doi:10.1186/2041-9139-5-12
686 Nong QD, Mohamad Ishak NS, Matsuura T, Kato Y, Watanabe H. 2017. Mapping the expression
687 of the sex determining factor Doublesex1 in *Daphnia magna* using a knock-in reporter. *Sci*
688 *Rep* **7**:13521. doi:10.1038/s41598-017-13730-4
689 OECD. 2022. Adverse Outcome Pathways, Molecular Screening and Toxicogenomics - OECD.
690 https://www.oecd.org/chemicalsafety/testing/adverse-outcome-pathways-molecular-
691 screening-and-toxicogenomics.htm
692 OECD. 2018. *Daphnia magna* Reproduction Test (OECD TG 211). Paris: OECD.
693 doi:10.1787/9789264304741-12-en
694 OECD. 2004. Test No. 202: Daphnia sp. Acute Immobilisation Test. Paris: Organisation for
695 Economic Co-operation and Development.
696 OpenSeadragon. An open-source, web-based viewer for high-resolution zoomable images,
697 implemented in pure Javascript, for desktop and mobile. [Accessed in 2020].
698 https://openseadragon.github.io/

Parr CS, Wilson N, Leary P, Schulz KS, Lans K, Walley L, Hammock JA, Goddard A, Rice J, Studer M, Holmes JTG, Corrigan, Jr. RJ. 2014. The Encyclopedia of Life v2: providing global access to knowledge about life on earth. *Biodivers Data J* e1079. doi:10.3897/BDJ.2.e1079

Quaglia A, Sabelli B, Villani L. 1976. Studies on the intestine of Daphnidae (Crustacea, Cladocera) ultrastructure of the midgut of *Daphnia magna* and *Daphnia obtusa*. *J Morphol* **150**:711–725. doi:10.1002/jmor.1051500306

Ramírez-Duarte W, Rondon Barragan I, Eslava-Mocha P. 2008. Acute toxicity and histopathological alterations of Roundup® herbicide on "cachama blanca" (*Piaractus brachypomus*). *Pesqui Veterinária Bras* **28**:547. doi:10.1590/S0100-736X2008001100002

Rossi F. 1980. Comparative observations on the female reproductive system and parthenogenetic oogenesis in Cladocera. *Bolletino Zool* **47**:21–38. doi:10.1080/11250008009440317

Sabaliauskas NA, Foutz CA, Mest JR, Budgeon LR, Sidor AT, Gershenson JA, Joshi SB, Cheng KC. 2006. High-throughput zebrafish histology. *Methods*, Zebrafish as a Model for Development **39**:246–254. doi:10.1016/j.ymeth.2006.03.001

Schultz TW, Kennedy JR. 1976. The fine structure of the digestive system of *Daphnia pulex* (Crustacea: Cladocera). *Tissue Cell* **8**:479–490. doi:10.1016/0040-8166(76)90008-2

Shaw JR, Pfrender ME, Eads BD, Klaper R, Callaghan A, Sibly RM, Colson I, Jansen B, Gilbert D, Colbourne JK. 2008. *Daphnia* as an emerging model for toxicological genomics In: Hogstrand C, Kille P, editors. Advances in Experimental Biology, Comparative Toxicogenomics. Elsevier. pp. 165–328. doi:10.1016/S1872-2423(08)00005-7

Smirnov NN. 2017. Physiology of the Cladocera: Second Edition, Physiology of the Cladocera: Second Edition.

Smith MJ, Weber RJM, Viant MR. 2022. Spatially mapping the baseline and Bisphenol-A exposed *Daphnia magna* lipidome using desorption electrospray ionization-mass spectrometry. *Metabolites* **12**:33. doi:10.3390/metabo12010033

Stein RJ, Richter WR, Zussman RA, Brynjolfsson G. 1966. Ultrastructural characterization of *Daphnia* heart muscle. *J Cell Biol* **29**:168–170.

Steinsland AJ. 1982. Heart ultrastructure in *Daphnia pulex* De Geer (Crustacea, Branchiopoda, Cladocera). *J Crustac Biol* **2**:54–58. doi:10.2307/1548112

Stollewerk A. 2010. The water flea *Daphnia* - a "new" model system for ecology and evolution? *J Biol* **9**:21. doi:10.1186/jbiol212

Tkaczyk A, Bownik A, Dudka J, Kowal K, Ślaska B. 2021. *Daphnia magna* model in the toxicity assessment of pharmaceuticals: A review. *Sci Total Environ* **763**:143038. doi:10.1016/j.scitotenv.2020.143038

US EPA. 2014. Next Generation Risk Assessment: incorporation of recent advances in molecular, computational, and systems biology (final report). https://cfpub.epa.gov/ncea/risk/recordisplay.cfm?deid=286690

Weiss LC, Tollrian R, Herbert Z, Laforsch C. 2012. Morphology of the *Daphnia* nervous system: a comparative study on *Daphnia pulex*, *Daphnia lumholtzi*, and *Daphnia longicephala*. *J Morphol* **273**:1392–1405. doi:10.1002/jmor.20068

Wester PW, Vos JG. 1994. Toxicological pathology in laboratory fish: an evaluation with two species and various environmental contaminants. *Ecotoxicol Lond Engl* **3**:21–44. doi:10.1007/BF00121386

Wuerz M, Huebner E, Huebner J. 2017. The morphology of the male reproductive system, spermatogenesis and the spermatozoon of *Daphnia magna* (Crustacea: Branchiopoda). *J Morphol* **278**:1536–1550. doi:10.1002/jmor.20729

Yakovlev MA, Vanselow DJ, Ngu MS, Zaino CR, Katz SR, Ding Y, Parkinson D, Wang SY, Ang KC, La Riviere P, Cheng KC. 2022. A wide-field micro-computed tomography detector: micron resolution at half-centimetre scale. *J Synchrotron Radiat* **29**. doi:10.1107/S160057752101287X

Zaffagnini F, Zeni C. 1987. Ultrastructural investigations on the labral glands of *Daphnia obtusa* (Crustacea, Cladocera). *J Morphol* **193**:23–33. doi:10.1002/jmor.1051930104

Zaffagnini F, Zeni C. 1986. Considerations on some cytological and ultrastructural observations on fat cells of *Daphnia* (Crustacea, Cladocera). *Bollettino di zoologia* **53**:33–39. doi:10.1080/11250008609355480

Zeni C, Franchini A. 1990. A preliminary histochemical study on the labral glands of *Daphnia obtusa* (Crustacea, Cladocera). *Acta Histochem* **88**:175–181.